

Novel Mixed Flow Air-Turbine for Bidirectional Operation in OWC Wave Energy Converters

C. Moisel, T.H. Carolus

*Institut für Fluid- und Thermodynamik, University of Siegen
57068 Siegen, Germany*

christoph.moisel@uni-siegen.de

thomas.carolus@uni-siegen.de

Abstract— A wide variety of turbine concepts with the capability of handling the bidirectional flow produced by an oscillating water column (OWC) wave energy converter have been proposed until today. Objective of this study is a detailed investigation of a novel mixed flow reaction turbine with an unstaggered blade cascade. This new conceptual design is thought to combine the advantages of the reaction turbines with unstaggered cascade currently in place; the well-known axial Wells turbine suggested in the 1970s by Wells and a radial turbine first suggested in the early 1980s by Sugihara.

A design strategy for the rotor including corrections for reducing secondary flows at the corners between blade and side walls, as well as design strategy for casing is introduced. Numerical RANS simulations are employed for manual optimization of the turbine. A first prototype is manufactured and performance tested. Eventually, a comparison of the present mixed flow turbine with a state-of-the-art axial Wells turbine with guide vanes and a radial turbine revealed a considerably increased capability of pneumatic power 'per unit rotor diameter and unit rotor speed' as well as significantly reduced sound emission for the mixed flow turbine.

Keywords— Oscillating Water Column, Wave Energy, Bidirectional, Air-Turbine, Mixed Flow, Wells Turbine

I. INTRODUCTION

The oscillating water column (OWC) system is one of the most promising and intensively studied principles of harnessing the energy from ocean waves. Within the last decades different types of turbines have been proposed for application in OWC devices [1-3]. These air turbines, capable of handling a bidirectional flow, can be categorized by their fundamental operational principle. They are either reaction or impulse type turbines [4]. Reaction turbines such as the axial-flow WELLS turbine require airfoil-type blades with their lift being a key parameter [5-7]. The relative flow in the rotor is accelerated and the pressure drop across the rotor is substantial. In contrast, impulse turbines require highly cambered rotor blades that deflect the relative flow without an essential acceleration [2, 8-13]; the pressure variation from rotor entrance to exit is small; the flow needs to be accelerated in guide vanes or nozzles.

Criteria for utilization of a specific turbine design for OWC-application are mechanical robustness, simplicity and compactness of its design, energy yield in a given and specified wave climate (hence in a wide range of operational conditions), and, after all, low noise emission.

Drawbacks of the well-known axial WELLS turbine [5], Fig. 1 (a), are its limited stall-free operating range and a comparably low peak efficiency [6, 14]. The spanwise variation of angle of attack of the flow to the unique non-staggered blades is regarded as the main reason.

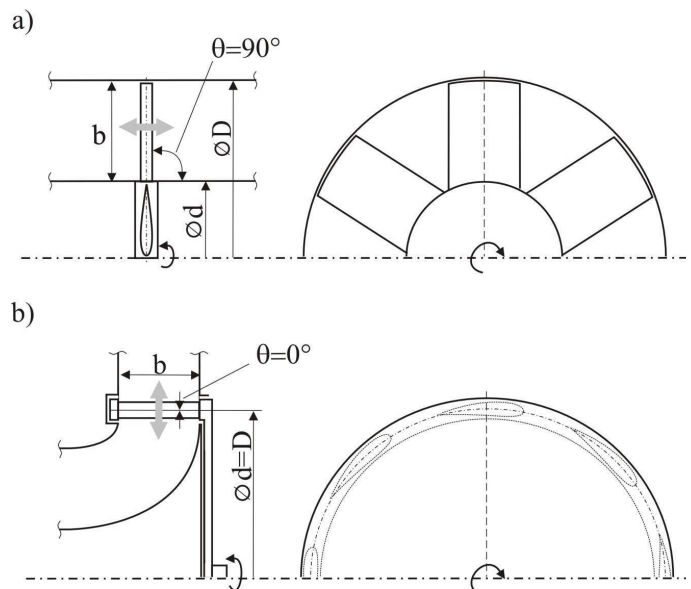


Fig. 1 Fixed-pitch reaction turbines for bidirectional flow: a) axial (Wells) turbine, b) radial turbine; D = nominal (tip) diameter, d = diameter at hub/rotor disc, b = width of blade channel, θ = angle of bladed cascade with respect to the rotor axis.

At first glance purely radial turbines, suggested in the early 1980s by SUGIHARA [15] and KENTFIELD [16], Fig. 1(b), promise higher peak efficiencies since the angle of attack to the blade can be kept constant. However, by the authors of this paper, huge differences in the volume flow rate vs. pressure head characteristics for both principal through flow directions as well as losses due to rotor disc friction were found to be limiting factors of the radial bidirectional turbine, [17].

The ideas underlying this present study are

- (i) reducing the spanwise variation of angle of attack of flow entering the bladed cascade due to the alignment of the blade cascade with an angle $\theta < 90^\circ$ and hence improving the stall margin
- (ii) reducing the diameter of the rotor disc $d < D$ and hence minimizing the disc friction losses
- (iii) increasing the meridional through flow area and hence the volume flow rate the turbine can take in.

These ideas result in a novel mixed flow (or diagonal) turbine that potentially excels the performance of a purely axial or radial design.

Objective of this paper is a detailed investigation of the mixed flow turbine concept. We introduce a design strategy for the rotor including corrections for reducing secondary flows at the corners between blade and side walls, as well as design strategy for the turbines casing. Numerical RANS simulations are employed for manual optimization of the turbine. A first prototype will be designed and manufactured for experimental performance testing. First experimental steady state characteristic curves will be presented. Eventually, in order to rate the performance achieved for the mixed flow turbine a comparison with a state-of-the-art axial Wells turbine with guide vanes and a radial turbine will be carried out.

II. MIXED FLOW TURBINE: LAYOUT AND MAIN PARAMETERS

The rotor of the mixed flow turbine comprises a number of blades placed between a rotor disc and a shroud, Fig. 2. The casing and the hub core guides the in- and outward flow.

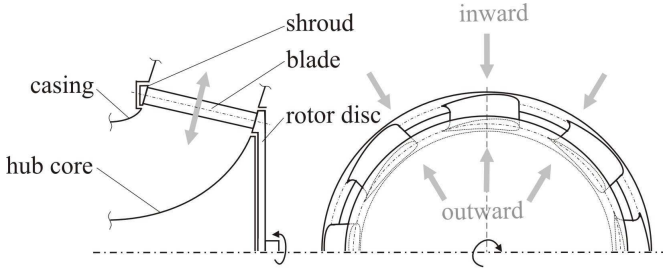


Fig. 2 Definitions and transformations of airfoils sections for the mixed flow rotor

The blades are non-staggered and are made of airfoil sections. To ensure a symmetric performance of the rotor blades, i.e. independent of inward and outward flow, lift and drag polars of the airfoil sections have to be the same for both flow directions. As the stream surfaces in the relative frame of reference are conical, the blades need to be mapped onto such a surface. This is why the airfoil section in Fig. 3 is seemingly cambered. Ideally the mapped blades encounter even in a

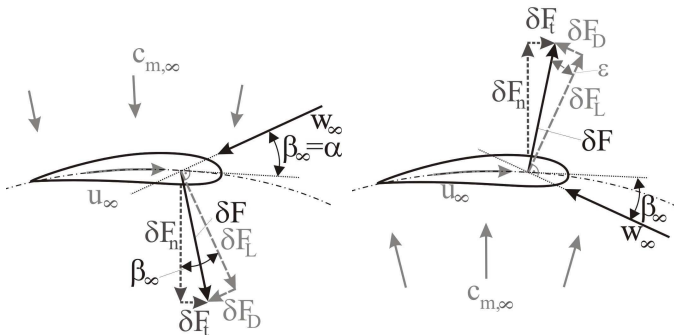


Fig. 3 Blade of mixed flow turbine (mapped onto conical surface); definition of vector-mean flow velocity w_∞ and flow direction β_∞ ; left: forces for inward flow, right: for outward flow

converging or diverging flow field the same angle of attack α which equals the mean angle β_∞ of the vector mean flow velocity $w_\infty = 0.5(w_1 + w_2)$. According to classic airfoil theory, this results in a tangential δF_t and a normal force δF_n given by

$$\delta F_t = \delta F_L \sin \beta_\infty - \delta F_D \cos \beta_\infty \quad (1)$$

$$\delta F_n = \delta F_L \cos \beta_\infty + \delta F_D \sin \beta_\infty \quad (2)$$

δF_t produces the desired rectified torque, ideally independent whether the flow is inward or outward.

A. Rotor

The characteristic dimensions of the mixed flow rotor are the nominal turbine diameter D , d at shroud and impeller disc, and the width b , Fig. 4. 'Nominal' refers to the blade mean line, not to the true diameter of the rotor.

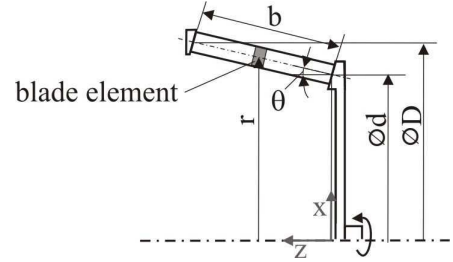


Fig. 4 Rotor of a mixed flow fixed-pitch reaction turbines for bidirectional flow: D = nominal diameter at shroud, d = diameter at rotor disc, b = width of blade channel, θ = angle of bladed cascade with respect to the rotor axis.

Due to the alignment of the rotors blades into a conical plane with $0^\circ < \theta < 90^\circ$ another degree of freedom for the rotor design can be utilized. In contrast to the axial rotor the through flow area can be increased by just increasing b . Fig. 5 illustrates the chord length and blade spacing

$$t = \frac{\pi r}{Z} \quad (3)$$

r is the local radius where a particular blade element is located at and Z is the number of blades.

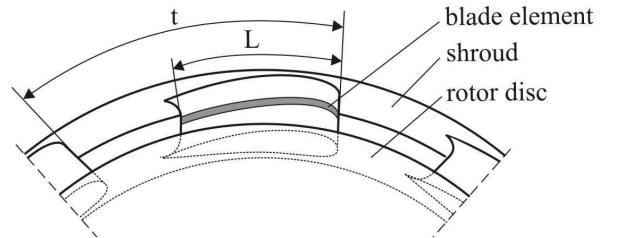


Fig. 5 Schematic layout of mixed flow rotor blade cascade in 3D view

Prior to mapping, each blade element is a section of a symmetrically shaped airfoil with chord length L , maximum thickness th and position of maximum thickness xd , Fig. 6.

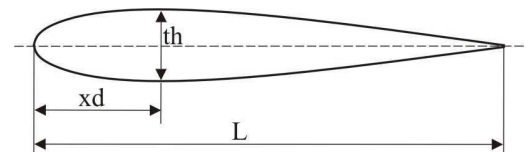


Fig. 6 Symmetric airfoil, L = chord length, xd = position of maximum thickness and th = maximum thickness

To map a blade element onto the conically shaped stream surface, three main transformations have to be performed, Fig. 7, see also [18]:

- (i) Rotating the blade element by an angle θ .
- (ii) As the streamlines in an axial turbine form a coaxial cylindrical surface, the blade elements of an axial cascade have to be mapped on the radius of the coaxial cylinder they are located, see e.g. [19]. Similarly, in the diagonal cascade one component of the flow field is also cylindrical; hence the blade element has to be mapped onto the resulting cylindrical surface; the relevant radius $r_{p,n}$ is the *normal* projection from the blade element to the rotors rotational axis.
- (iii) Then the blade element has to be mapped onto the circumference; here the relevant radius is $r_{p,i}$; for details see e.g. [20].

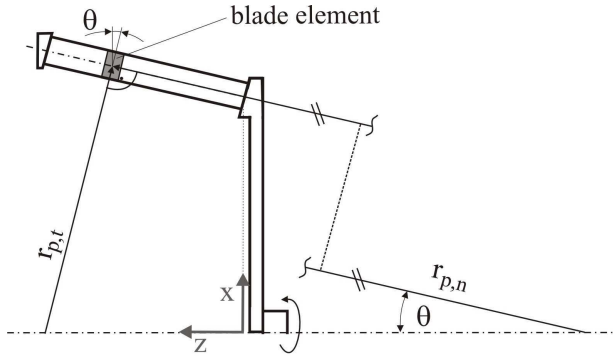


Fig. 7 Definition of the relevant blade properties for blade element transformation into the diagonal rotor plane

In a former study the authors showed that the three-dimensional boundary layer at the corners between blade and side walls may ruin the flow over the blade. To reduce these effects sidewall correction and blade fitting methods are incorporated. For that the blade is divided into three main sections over span: two sections in vicinity of the corners and a middle section, as depicted schematically in Fig. 8. Four planes (I-IV) are defined for description of the full geometry. The resulting rotor blade is presented in Fig. 8.

B. Casing

The casing of a mixed flow turbine is more complex than e.g. for an axial turbine. Fig. 9 shows a generic casing comprising three main sections:

- The core section between the inside and outside planes I_i and I_o
 - An optional radial section between I_o and II_o
 - An optional axial section confined by the planes I_i and II_i ; essential part is the hub core.
- Further measures are depicted in Fig. 9.

III. METHODOLOGY

A. General strategy

A tool was implemented which enables generating geometries of the rotor and the casing for arbitrary values of the parameters introduced in the previous chapter. Some parameters were adopted from rules applied for designing other turbo machines. Numerical flow simulation (RANS) was employed for assessing the result in terms of integral performance parameters and local details of the flow. This enabled a step-by-step improvement of the overall design. Eventually a model of the

most promising turbine was manufactured and experimentally performance tested.

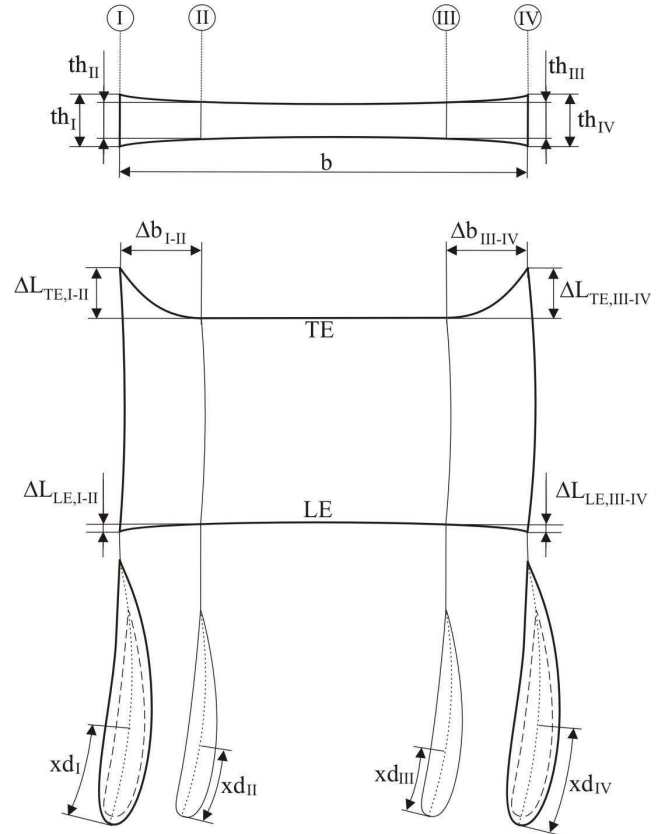


Fig. 8 Definition of mixed flow rotor blade properties with side wall correction

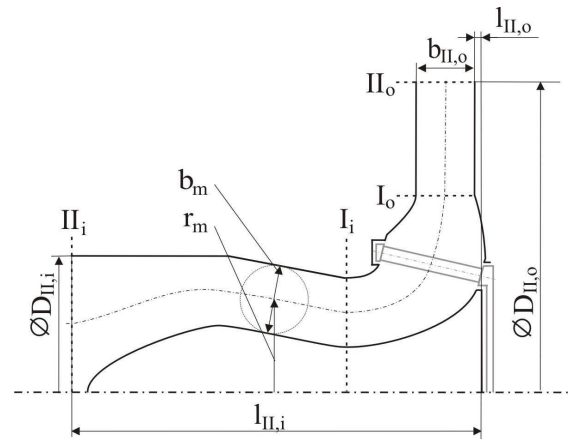


Fig. 9 Schematic meridional view of the mixed flow turbine

B. Numerical Setup

The flow in the mixed flow turbine is simulated using the commercial 3D Navier-Stokes code ANSYS CFX™ with the standard SST-turbulence-model [21] and the ‘high resolution advection scheme’ [22]. In the composite computational domain (Fig. 10) the steady, incompressible, three-dimensional Reynolds-averaged Navier-Stokes (RANS) equations are solved in a rotating reference frame. The block-structured numerical grid, prepared using ANSYS TurboGrid™ consists of about 2.5 million nodes. Common grid quality criteria were considered; for instance the grid angles are at least above 21°. The maximum value of y^+_{max} for the first node adjacent to the blade surface (of rotor and stator) was set in TurboGrid™ to

$y^+ < 1$ at a Reynolds Number $Re = 3.7e5$, a suitable mesh resolution out of a mesh refinement study. Steady state solutions are then obtained in the reference frame [22].

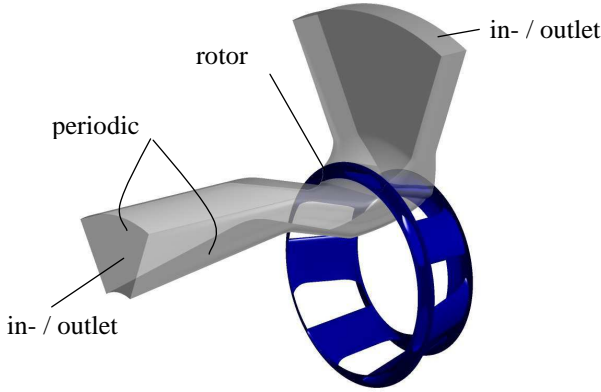


Fig. 10 Numerical domain of mixed flow turbine

Due to the turbine symmetry, only one blade annulus was modelled and 1:1 periodic boundary conditions were imposed in the circumferential direction. An inlet normal mass flow rate was imposed on the respective upstream boundary for each flow direction; an area averaged static pressure at the corresponding downstream boundary. Note that within this study there is no tip or duct clearance modelled in the computational domain. Convergence was evaluated by monitoring the integral performance parameters, e.g. blade torque.

C. Experimental Setup

The bidirectional aero-acoustic steady state test rig at University of Siegen designed according to the guidelines for fan performance testing in ISO 5801 [23] is depicted schematically in Fig. 11. The volume flow rate through the facility and hence the turbine to be tested is supplied by a centrifugal fan. Its adjustable speed drive allows setting any value of the volume flow rate. The flow direction is determined by the position of a large two way directional control valve, located close to the fan. The volume flow rate is measured by means of a symmetric Venturi nozzle. The complete airflow supply unit and flow path involves various sound attenuator measures to prevent acoustic radiation from the fan drive and auxiliary devices into the laboratory environment as well as to the flow path to the turbine avoiding background noise tamper the turbines noise emissions measured. The large chamber contains screens and honeycombs for reduction of swirl and turbulence reduction in pressure side operation of the rig. The gauge pressure in the chamber is positive when the test rig is installed at the inlet side (is) of the turbine and negative for outlet side (os) operation. The opposite port of the turbine is always connected to the free laboratory atmosphere.

The test facility allows direct measurement of total to static pressure head Δp_{ts} , volume flow rate V , density ρ , shaft torque T and rotational speed n . It should be stated explicitly that the torque measurement technique, using a telemetric torque flange connecting turbine rotor and generator shaft directly, allows the measurement of the pure aerodynamic torque without any mechanical losses ($\eta_{mech} = 100\%$). Beside the aerodynamic measurements also acoustic sound pressure and even the acoustic sound power of the turbine can be determined following DIN EN ISO 3741 [24]. Prior to the turbine test a calibrated reference sound source (RSS) is placed

at the position of the turbine. The known sound power of the reference sound is recorded by a microphone.

More detailed information on the test procedure and layout of the test rigs instrumentation, including: a validation of the test rigs ability for equal bidirectional measurements as well as the steady state measurement method in general, the calibration process of the flow rate measurement, sample rates and data analysis process, a comprehensive uncertainty specification of the instrumentation and analysis of random and bias errors within the measurement process are compiled in [25]. The uncertainties involved in the measurements of the mixed flow turbine are given in Appendix C.

IV. DESIGN OF TURBINE

A. Fixed Parameters

Some parameters have been fixed before starting the turbine design:

- The rotors nominal diameter was chosen as $D = 0.35$ m due to the limited capability of five-axis milling machine at the workshop.
- The rotational speed of the rotor is $n = 4000$ rpm which corresponds to circumferential Mach number

$$Ma \equiv \frac{u_D}{a} = 0.21.$$

- Ma is defined with the speed of sound a and the rotational velocity u_D at the nominal rotor diameter which is - for cascades with small deflection - in the same order of magnitude as the relative flow velocity w_∞ to the blades.
- The diameter of the casing at plane Π_i (Fig. 9) is $D_{\Pi,i} = 0.4$ m.

B. Design philosophy

Rotor. The goals within the manual optimization process are a maximization of the bladed through flow area $A = \pi/2 \cdot (D+d) \cdot b$ while maintaining a limited spanwise variation of the angle of attack to the blades. This was achieved by varying D , d , b and hence θ .

Blade cascade. For the blade cascade the solidity at the rotor disc

$$\sigma \equiv \frac{L}{t} \quad (4)$$

was chosen as approximately 0.6. This is a typical value for existing reaction turbines, see e.g. [6, 20]. The aspect ratio

$$\gamma \equiv \frac{b}{L}, \quad (5)$$

is required to be at least 1.5 to minimize side wall effects. The value of the Reynolds number

$$Re_L \equiv \frac{Lu_D}{\nu} = 370.000 \quad (6)$$

aimed at is assumed to be supercritical [4, 26]. Re_L is determined with the circumferential velocity at the rotor's nominal diameter D and the kinematic viscosity of the air ν .

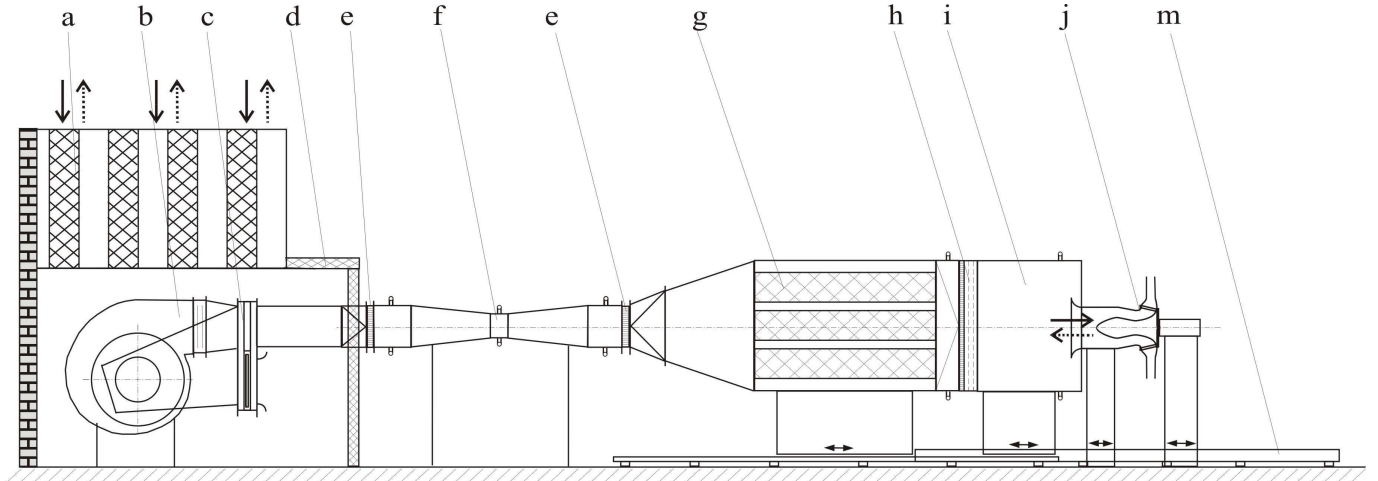


Fig. 11 Bidirectional test facility at the University of Siegen: a) splitter attenuator, b) centrifugal fan, c) flow diverter (two way directional flow control valve), d) acoustic enclosure, e) honeycombs, f) calibrated Venturi nozzle, g) splitter attenuator, h) honeycombs and turbulence control screens, i) chamber, j) model turbine, m)° linear track

Blade. Different kinds of airfoils were tested along the span to achieve a good compromise between high blade efficiency and capability of tolerating high angles of attack before stalling. In this study airfoils of the four digit NACA series were chosen. The types with a maximum thickness between 12% and 21% of chord length have been employed in many studies for use in unstaggered cascades, see e.g. [6, 7]. Note that thin airfoils of these types have a high lift-to-drag ratio, whereas the thicker types can cope with high angles of attack.

Additional attention was given to the corner regions where a blade meets the side wall. Side wall corrections were achieved by near-wall modifications of chord length, blade thickness and position of maximum thickness. For details see the Appendix A & B.

Casing. We refer to Fig. 9: The main task of the core section between the inside and outside planes I_i and I_o is to deflect the flow from axial into radial direction or vice versa, not its acceleration or deceleration.

For outward flow the radial section between I_o and II_o should act as a classical radial diffuser; for inward flow it should provide a low-loss acceleration of the incoming fluid.

The axial section confined by the planes I_i and II_i is an axial diffuser or nozzle; the changes of cross-sectional area along the flow path are controlled by the contours of the casing and the hub core.

A preliminary hint for preventing flow separation was derived from the theories by MELDAU [27] and STRSCHELETZKY [28]. The ratio of through flow and circumferential flow velocity c_m/c_u is considered as a criterion. Two options had been investigated: (i) manipulate c_m and hence acceleration of the flow, or (ii) limit c_u by increasing the mean radius r_m where the flow is guided.

C. Results

Rotor. The rotor obtained by the numerically aided optimization is depicted in Fig. 13a. Its main design parameters are compiled in Table I.

Casing. The detailed layout of the mixed flow turbines casing is depicted in Fig. 12. The black dashed line indicates the location of the blade cascade, the core section for flow deflection is coloured in red and the axial and radial sections be-

tween planes I and II are coloured in blue. The radial section consists of simply parallel walls, whereas in the entire axial section an outstretched hub core assists the flow to prevent flow separation.

TABLE I
ROTOR AND BLADE DESIGN PARAMETER

Main rotor / flow parameters				
D [m]	0.35			
d/D [-]	0.8			
b/D [-]	0.35			
A^* [-]	1.26			
Re_L [-]	3.7e5			
Ma_u [-]	0.21			
Airfoil and cascade geometry at planes I - IV without side wall corrections				
Plane	I	II	III	IV
NACA	0018	0015	0015	0018
L/D [-]	0.22	0.22	0.22	0.22
xd/L [-]	0.3	0.3	0.3	0.3
σ [-]	0.62	0.58	0.52	0.49
Airfoil and cascade geometry at planes I - IV with side wall corrections (final design)				
Plane	I	II	III	IV
L/D [-]	0.25	0.22	0.22	0.27
xd/L [-]	0.6	0.3	0.3	0.6
σ [-]	0.72	0.58	0.52	0.61
A rotor disc region		at shroud region		
$\Delta b_{r,iv}/L$ [-]	0.34	$\Delta b_{III-IV}/L$ [-]	0.38	
$\Delta h_{r,iv}/L$ [-]	0	$\Delta h_{III-IV}/L$ [-]	0	
$\Delta LE_{r,iv}/L$ [-]	0	$\Delta LE_{III-IV}/L$ [-]	0	
$\Delta TE_{r,iv}/L$ [-]	0.16	$\Delta TE_{III-IV}/L$ [-]	0.24	

The main dimensions of the casing according to the definitions introduced in Fig. 9 are compiled in Table II. The final CAD model of the full turbine is depicted in Fig. 13b.

TABLE II
MAIN DESIGN PARAMETER OF THE CASING

$D_{II,r}/D$ [-]	1.14	$D_{II,o}/D$ [-]	2.5
$b_{II,r}/D$ [-]	-	$b_{II,o}/D$ [-]	0.16
$l_{II,r}/D$ [-]	1.64	$l_{II,o}/D$ [-]	0.05

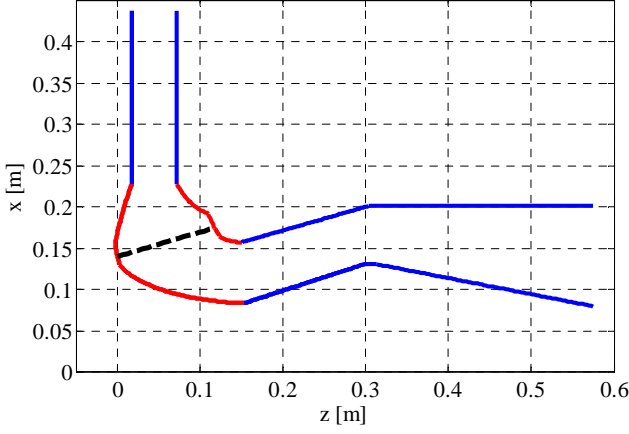


Fig. 12 Meridional view of the mixed flow turbines casing

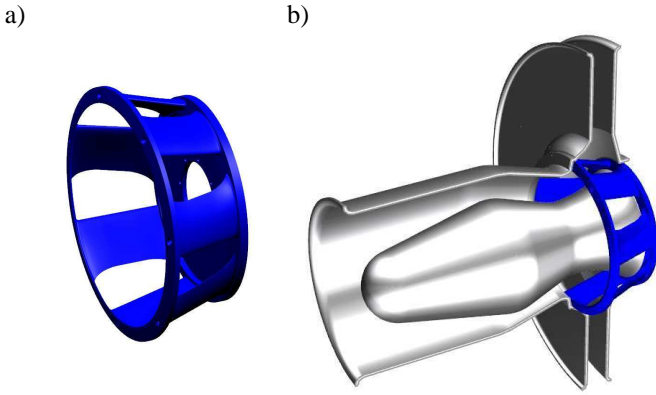


Fig. 13 CAD-models: a) mixed flow rotor with side wall corrections, b) mixed flow turbine

D. Manufacture

The complete turbine assembly on the test rig is presented in Fig. 14.

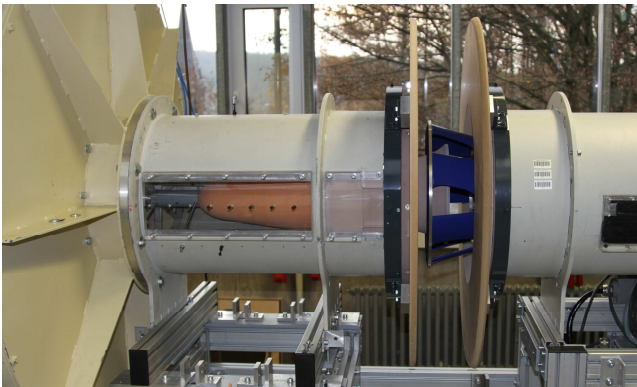


Fig. 14 Mixed flow turbine assembled on the test rig

V. PERFORMANCE OF TURBINE

A. Coefficients and Performance Parameters

The aerodynamic performance characteristics of the mixed flow turbine are described in terms of the pressure coefficient

$$\psi_{ts} \equiv \Delta p_{ts} / \left(\frac{\pi^2}{2} \rho D^2 n^2 \right), \quad (7)$$

the flow rate coefficient

$$\phi \equiv V / \left(\frac{\pi^2}{4} D^3 n \right), \quad (8)$$

and the power coefficient

$$\lambda \equiv T \omega / \left(\frac{\pi^4}{8} \rho D^5 n^3 \right). \quad (9)$$

Δp_{ts} is the total to static pressure drop, V the volume flow rate, T the torque, ρ the local density, D the nominal rotor diameter, n the rotational speed, and ω the angular velocity. Finally, the efficiency is

$$\eta \equiv \lambda / \phi \psi. \quad (10)$$

The acoustic emissions of turbines are described by two different definitions of a specific sound power level. Both are based on the scaling law for the acoustic power P_{ac} of fans which has been proposed by MADISON [29]:

$$P_{ac} \sim u_{tip}^\gamma D_{tip}. \quad (12)$$

Madison's law can be transformed to normalize the acoustic power emitted by a machine by its pneumatic power V and Δp and hence is used to compare different machine types. If $\gamma = 5$ is assumed (an average value found appropriate for the Wells turbine [6]), this results - in terms of sound power levels - in

$$L_{w,spec} \equiv L_w - 10 \lg \frac{V}{V_0} - 20 \lg \frac{\Delta p_{ts}}{\Delta p_0} \quad (13)$$

with the reference pressure $\Delta p_0 = 1 \text{ Pa}$ and the reference flow rate $V_0 = 1 \text{ m}^3/\text{s}$.

Madison's scaling law (Eq. (12)) can also be employed to normalize the overall sound power emitted from geometrically scaled-up or scaled-down machines at different rotational speeds. A dimensional analysis results in the non-dimensional acoustic power

$$P_{ac}^* \sim \frac{P_{ac}}{u_{tip}^3 D_{tip}^2 \rho}. \quad (14)$$

This yields in the second definition of a specific sound power level

$$L_{w,spec^*} \equiv L_w - 10 \lg \left(\frac{u_{tip}^3 D_{tip}^2 \rho M a_{u,tip}^{(\gamma-3)}}{P_0} \right) \quad (15)$$

with the acoustic reference power $P_0 = 1 \text{ e}^{-12} \text{ W}$ and the empirical Mach number exponent γ , which again is assumed to be 5.

B. Experimentally determined characteristic curves

The aero-acoustic steady state characteristics of the turbine are displayed in Fig. 15. As typical for most reactions turbines,

the pressure drop ψ_{ts} increases approximately linearly with ϕ . The minor divergence in slope between outward (out) and inward (in) can be tracked back to the difference in pressure recovery between axial and radial sections located downstream of the rotor. The flow direction effects as well the maximum power ('mp') produced before stall occurs (sharp drop of λ). A small hysteresis loop is observed when decreasing ϕ after stall has occurred on the blade, indicated by the dashed lines and highlighted exemplarily by the black arrows for the 'in' curve of λ .

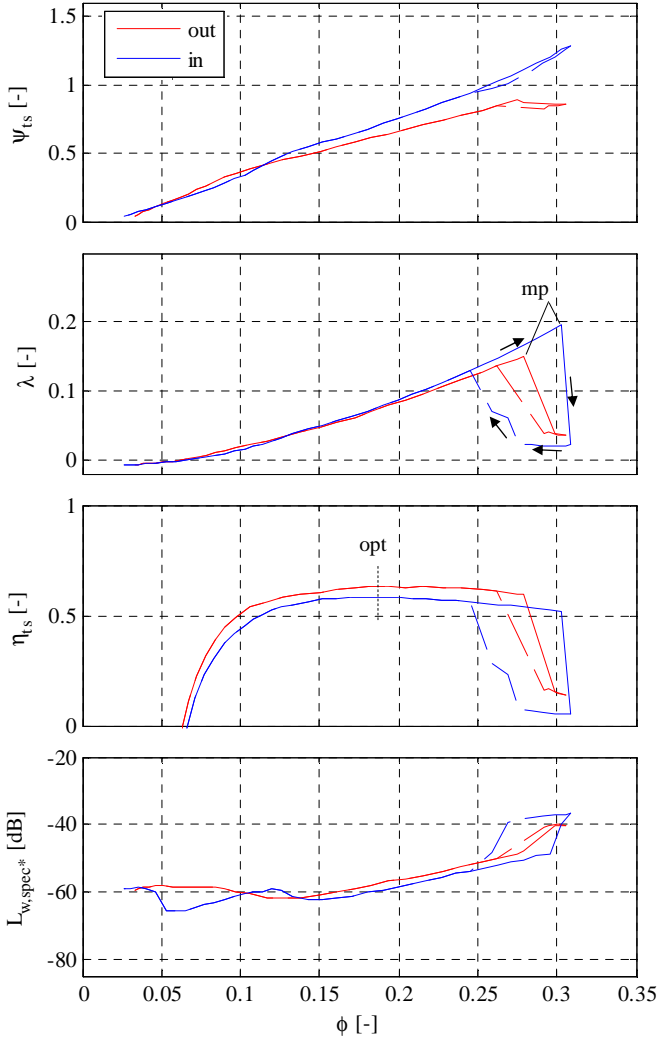


Fig. 15. Measured steady state characteristic curves of the mixed flow turbine (the solid lines indicate a variation of flow rate from 0 to a maximum value, the dashed lines the reverse)

Hysteresis occurs generally due to secondary flow effects on the suction side of the blade, preventing the flow to reattach to the blade directly after stall. The difference in efficiency to be observed can be traced back to the limited axial diameter $D_{II,i}$ at the connection to the test rig and hence high kinetic energy losses at the exit in 'in' flow direction. The specific sound power level as a function of ϕ is approximately equal for both through flow directions. The stall event can be detected by the steep rise in sound level by about 12 dB.

C. Comparison with other fixed-pitch reaction turbines

In order to rate the results achieved here for the mixed flow turbine, a comparison to other state-of-the-art axial and radial fixed-pitch reaction turbines is carried out. The selected turbines are the axial Wells turbine design with best peak efficiency out of study [6], design 'R1' combined with guide vanes 'GV6' and the radial turbine investigated by these authors in study [17], see Fig. 16. The main geometric and aerodynamic parameters of the axial and radial turbine are compiled in Table III. The relevant parameters for the mixed flow turbine are to be found in Table I. The solidity σ at the hub or respectively at the rotor disc is for all three turbines approximately equal. Also the Reynolds and Mach numbers are in the same range.

It is still an ongoing discussion how to compare the performance data of different turbines designs, especially when they are not designed for the same application (OWC's pressure vs. flow-rate characteristic (damping)). We try to overcome these specific issues by plotting the turbines characteristic curves over the specific pneumatic energy supply in terms of $\phi * \psi_{ts}$. Fig. 17 shows the characteristics of all turbines. Obviously the novel mixed flow turbine can transform significantly more pneumatic power into mechanical power 'per turbines diameter and speed' as compared to the other designs. Here again also the hysteresis characteristics of the turbines are indicated by the dotted lines. Visibly for the Wells and the mixed flow turbine hysteresis after stall can be detected, not being present for the radial turbine.

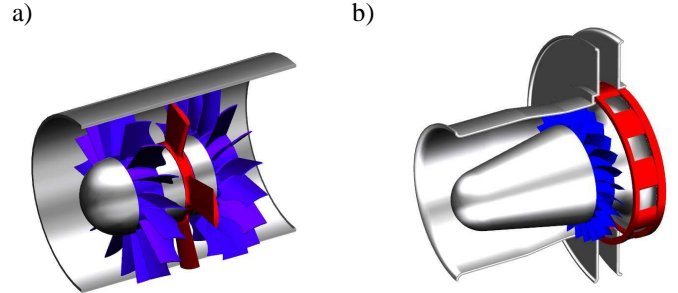


Figure 16. 3D models: a) Wells turbine with guide vanes [6], b) radial turbine [17]; rotor – red, guide vanes – blue

TABLE III
MAIN GEOMETRIC AND FLOW PARAMETERS OF TURBINES

Axial (Wells)		Radial	
D [m]	0.4	D [m]	0.4
d/D [-]	0.43	d/D [-]	1.0
b/D [-]	0.285	b/D [-]	0.14
A^* [-]	0.81	A^* [-]	0.56
σ_{hub} [-]	0.65	σ [-]	0.56
Re_L [-]	$5.2e5$	Re_L [-]	$4.2e5$
Ma_u [-]	0.24	Ma_u [-]	0.24

The black dash-dotted line in the λ graph indicates the theoretical limit (lim) for power conversion (energy input equals energy output). At the same time the sound emissions of the mixed flow turbine are significantly lower compared to both other turbines.

The power density of turbines can be traced back to the bladed through flow area which is inherently different for all designs because of geometrical reasons. We define a normalized bladed through flow area

$$A^* = \frac{\pi(D+d)b}{\frac{\pi D^2}{4}} = 2 \left(1 + \frac{d}{D}\right) \frac{b}{D}. \quad (16)$$

Because of the unavoidable hub axial rotors have always $A^* < 1$, here 0.81. For the radial or diagonal rotor the A^* can well be larger than 1. The mixed flow turbine has $A^* = 1.26$. This large through flow area is a unique feature of this turbine design.

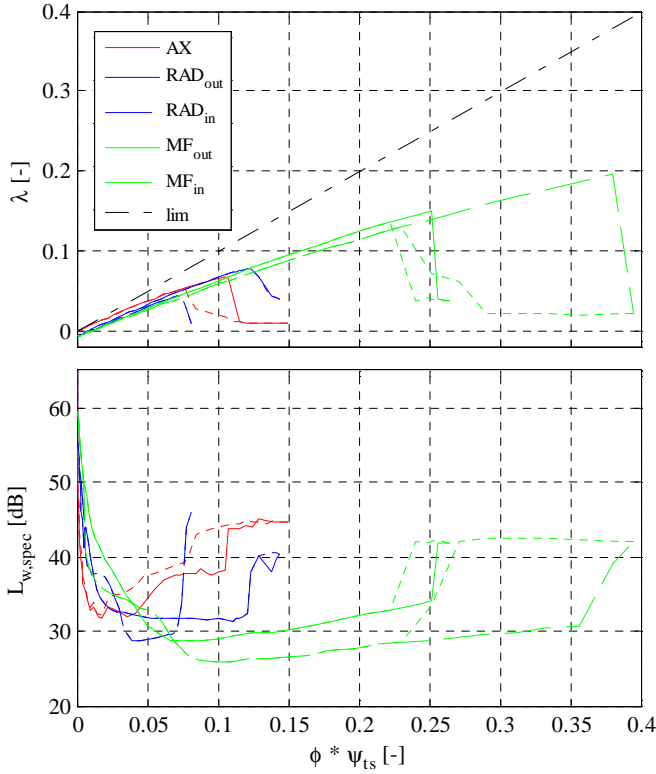


Figure 17. Measured steady state characteristic curves of axial (AX) [6], radial (RAD) [17] and present mixed flow (MF) turbine

VI. CONCLUSIONS AND OUTLOOK

A novel mixed flow reaction turbine for use in bidirectional flows has been presented. A design strategy for the rotor including corrections for reducing secondary flows at the corners between blade and side walls, as well as design strategy for the turbines casing have been introduced. Numerical RANS simulations have been employed for manual optimization. A first prototype has been manufactured and performance tested. Eventually, a comparison of the mixed flow turbine with a state-of-the-art axial Wells turbine with guide vanes and a radial turbine has been carried out. The comparison reveals that the mixed flow turbine design has a considerably increased capability of pneumatic power 'per unit rotor diameter and unit rotor speed' as well as significantly reduced sound emission as compared to the axial Wells and the radial turbine.

Due to the simply shaped casing the residual discharge energy which is wasted at the turbines exit, is high. A release of the geometrical constraints specified in this study point towards design as depicted in Fig. 18. Both designs are thought to real-

ize an improved total to static conversion efficiency as compared to the casing design presented in this study.

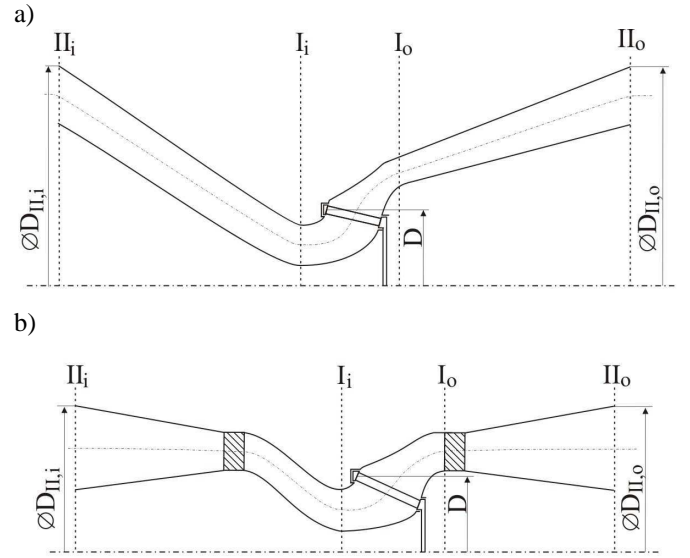


Fig. 18. Schematic meridional views of enhanced bidirectional turbines (based on the mixed flow rotor described in the present study); (a) casing with outstretched diagonal flow channels, (b) casing with guide vanes (hatched)

ACKNOWLEDGMENT

This work is supported by the German Federal Ministry for the Economics and Energy (BMWi) and Voith Hydro (FKZ 0325396). The authors greatly appreciate this support.

REFERENCES

- [1] A. F. O. Falcão and L. M. C. Gato, "Air Turbines," in *Comprehensive Renewable Energy*. vol. 8, A. Sayigh, Ed., ed Oxford: Elsevier, 2012, pp. 111-149.
- [2] T. Setoguchi, S. Santhakumar, H. Maeda, M. Takao, and K. Kaneko, "A review of impulse turbines for wave energy conversion," *Renewable Energy*, vol. 23, pp. 261-292, 2001.
- [3] T. Setoguchi and M. Takao, "Current status of self rectifying air turbines for wave energy conversion," *Energy Conversion and Management*, vol. 47, pp. 2382-2396, 2006.
- [4] S. L. Dixon and C. A. Hall, *Fluid Mechanics and Thermodynamics of Turbomachinery*, 6th ed. Boston: Butterworth Heinemann, 0-7506-7059-2, 2010.
- [5] A. A. Wells, "Fluid driven rotary transducer," British Patent Spec No. 1595700., 1976.
- [6] R. Starzmann, *Aero-Acoustic Analysis of Wells Turbines for Ocean Wave Energy Conversion* vol. 7. Duesseldorf: VDI, 978-3-18-350007-9, 2012.
- [7] S. Raghunathan, "The Wells air turbine for wave energy-conversion," *Progress in Aerospace Sciences*, vol. 31, pp. 335-386, 1995.
- [8] B. Pereiras, F. Castro, A. e. Marjani, and M. A. Rodríguez, "An improved radial impulse turbine for OWC," *Renewable Energy*, vol. 36, pp. 1477-1484, 2011.
- [9] B. Pereiras, D. Montoya, F. Castro, A. de la Villa, A. El Marjani, and M. A. Rodríguez, "Conception of a radial impulse turbine for an oscillating water column (OWC)," presented at the 3rd International Conference on Ocean Energy, Bilbao, Spain, 2010.
- [10] Y. Shpolyanski, I. N. Usachev, B. Istorik, and V. Sobolev, "The new orthogonal turbine for tidal, wave and low-head hydro power plants," *Supplement to International Journal on Hydropower (Marine Energy)*, vol. 6, pp. 10-14, 2009.
- [11] M. E. McCormick, J. G. Rehak, and B. D. Williams, "An experimental study of a bidirectional radial turbine for pneumatic wave energy conversion," in *Mastering Ocean through Technology*, Newport, Rhode Island, 1992, pp. 866-870.

- [12] T. Setoguchi, S. Santhakumar, M. Takao, T. H. Kim, and K. Kaneko, "A performance study of a radial turbine for wave energy conversion," *Proceedings of the Institution of Mechanical Engineers, Part A: Journal of Power and Energy*, vol. 216, pp. 15-22, February 1, 2002 2002.
- [13] A. Thakker, F. Hourigan, T. S. Dhanasekaran, M. E. Hemry, Z. Usmani, and J. Ryan, "Design and performance analysis of impulse turbine for a wave energy power plant," *International Journal of Energy Research*, vol. 29, pp. 13-36, 2005.
- [14] M. Suzuki and C. Arakawa, "Numerical simulation of 3-D stall mechanism on wells turbine for wave-power generating system," *International Journal of Offshore and Polar Engineering*, vol. 11, pp. 315-320, Dec 2001.
- [15] M. Sugihara, E. Morishita, T. Hirai, and S. Sekiya, "Turbine rotatable in one direction in a reciprocating flow," United Kingdom Patent GB2125113 A, 1984.
- [16] J. A. C. Kentfield, "A bi-flow directional air-turbine for wave energy extraction," in *6. International conference on alternative energy sources*, Miami Beach, FL, USA, 1983, pp. 59-60.
- [17] C. Moisel and T. H. Carolus, "Experimental loss analysis on a model-scale radial bidirectional air-turbine for wave energy conversion," presented at the 1st International Conference on Renewable Energies Offshore (RENEW), Lisbon, Portugal, 2014.
- [18] H. Kebschull, "Parametrische Geometriegenerierung der Beschaukelung von auftriebsbasierten Wellenenergeturbinen," Bachelor Thesis, Institut für Fluid- und Thermodynamik, University of Siegen, Siegen, 2015.
- [19] T. Carolus, *Ventilatoren* vol. 2. Stuttgart [u.a.] Teubner ISBN: 3-519-00433-X, 2009.
- [20] C. Moisel and T. H. Carolus, "Radial lift-based cascade for bidirectional Wave Energy Air-Turbines," in *ASME Turbo Expo 2014*, Düsseldorf, Germany, 2014.
- [21] F. R. Menter, "Two-equation eddy-viscosity turbulence models for engineering applications," *AIAA Journal*, vol. 32, pp. 1598-1605, August 1994 1994.
- [22] ANSYS, "ANSYS CFX-Solver Modeling Guide, Release 14.5," ed. Canonsburg, Pennsylvania, 2013.
- [23] ISO 5801, "Industrial fans - Performance testing using standardized airways," in *ISO 5801*, I.-I. O. f. Standardization, Ed., ed: BSi British Standards, 2007, p. 242.
- [24] DIN EN ISO 3741, "Bestimmung der Schalleistungspegel von Geräuschquellen aus Schalldruckmessungen - Hallraumverfahren der Genauigkeitsklasse 1," in *DIN EN ISO 3741* vol. DIN EN ISO 3741, D. I. f. n. e.V., Ed., ed. Berlin, Germany: Beuth Verlag, 2001, p. 24.
- [25] C. Moisel and T. Carolus, "A Facility for Testing the Aerodynamic and Acoustic Performance of Bidirectional Air Turbines for Ocean Wave Energy Conversion," *Eingereicht für das Journal of Renewable Energy*, 2015.
- [26] M. Takao, A. Thakker, R. Abdulhadi, and T. Setoguchi, "Effect of blade profile on the performance of a large-scale Wells turbine for wave-energy conversion," *International Journal of Sustainable Energy*, vol. 25, pp. 53-61, 2006.
- [27] E. Meldau, "Drallströmung im Drehholraum," Phd., Technische Hochschule Hannover, Hannover, 1935.
- [28] M. Strscheletsky, "Gleichgewichtsformen der rotationssymmetrischen Strömungen mit konstantem Drall in geraden, zylindrischen Rotationshöhlräumen," *Voith Forschung und Konstruktion*, vol. H. 5, October 1959 1959.
- [29] R. D. Madison, *Fan Engineering (Handbook)*, 5th Edition ed. Buffalo, N.Y.: Buffalo Forge Company, 1949.
- [30] R. L. Simpson, "JUNCTION FLOWS," *Annual Review of Fluid Mechanics*, vol. 33, pp. 415-443, 2001.
- [31] H. Schlichting and K. Gersten, *Grenzschichttheorie* vol. 10. Berlin Heidelberg: Springer-Verlag, ISBN: 3540230041, 2006.
- [32] J. M. Délerly, "Robert Legendre and Hanri Werlé: Toward the Elucidation of Three-Dimensional Separation," *Annu. rev. Fluid. Mech.*, vol. 33, pp. 129-154, 2001.
- [33] P. R. Ashill, J. L. Fulker, and K. C. Hackett, "A review of recent developments in flow control," *The Aeronautical Journal* vol. 109, pp. 205-232, 2005.
- [34] E. M. Greitzer, C. S. Tan, and M. B. Graf, *Internal Flow - Concepts and Applications*. Cambridge, UK: Cambridge University Press ISBN 0-521-34393-3, 2004.
- [35] G. A. Zess and K. A. Thole, "Computational Design and Experimental Evaluation of Using a Leading Edge Fillet on a Gas Turbine Vane," *Journal of Turbomachinery* vol. 124, pp. 167-175, 2002.
- [36] Ö. H. Turgut and C. Camci, "INFLUENCE OF LEADING EDGE FILLET AND NONAXISYMMETRIC CONTOURED ENDWALL ON TURBINE NGV EXIT FLOW STRUCTURE AND INTERACTIONS WITH THE RIM SEAL FLOW," in *Proceedings of ASME Turbo Expo 2013: Turbine Technical Conference and Exposition*, San Antonio, Texas, USA 2013.
- [37] C. Li, Z. Ye, and G. Wang, "Simulation of Flow Separation at the Wing-Body Junction with Different Fairings," *Journal of Aircraft*, vol. 45, pp. 258-266, 2008.
- [38] A. Beyene and T. Ireland, "Flexible turbine blade," US Patent No. 20050271508 A1, 2004.
- [39] H. Sauer, R. Mueller, and K. Vogeler, "Reduction of Secondary Flow Losses in Turbine Cascades by Leading Edge Modifications at the Endwall," *Journal of Turbomachinery* vol. 123, pp. 207-213, 2001.
- [40] N. Subramaniam, "Numerical Investigation of Endwall Contouring in a radial Bidirectional Turbine Cascade for Wave Energy Conversion," Master, Institut für Fluid- und Thermodynamik, University of Siegen, Siegen, 2014.
- [41] R. Arlitt, H. Bronowski, J. Weilepp, M. Engelhardt, and R. Starzmann, "Wells turbine having passive rotor blade displacement," US20110103958 A1, 2007.
- [42] K. Eden and H. Gebhard, *Dokumentation in der Mess- und Prüftechnik. Messen - Auswerten - Darstellen Protokolle - Berichte - Präsentationen*: Springer Vieweg 2014.
- [43] DIN 1319-3, "Grundlagen der Messtechnik - Auswertung von Messungen einer einzelnen Meßgröße, Messunsicherheiten," vol. DIN 1319-3, DIN Deutsches Institut für Normung e.V., Ed., ed. Berlin, Germany: Beuth Verlag, 1996.
- [44] DIN 1319-4, "Grundlagen der Messtechnik - Auswertung von Messungen, Messunsicherheiten," vol. DIN 1319-4, DIN Deutsches Institut für Normung e.V., Ed., ed. Berlin, Germany: Beuth Verlag, 1999.

APPENDIX

A. Corner flow phenomena

The detection of significant boundary layer interaction at corners between blade and side walls leading to secondary flow and flow separation effects reducing the rotors efficiency and operating range already found by these authors for the radial turbine, see e.g. [20] have motivated a further investigation of this phenomena. The effects of boundary layer interactions at the corners of almost vertical wall junctions are widely known to cause outstretched swirl structures (known as e.g. horseshoe vortex) and flow separation (known as e.g. corner stall) [30]. Kinetic energy deficits due to the boundary layers of wall and blade encountering almost vertically, together with the flow deceleration along an airfoil downstream of its position of maximum thickness are the cause for these effects [31]. A comprehensive overview on three dimensional flow separation phenomena can be found in [32]. Many studies have carried out to suppress these phenomena by either active or passive flow control methods [33, 34]. In turbo machinery and aircraft (passive) adapted geometrical side wall correction methods at blades/wings – fillets (see e.g. [35, 36]) or fairings (see e.g. [37]) and adjacent walls/fuselage - end wall contouring (see e.g. [38, 39]) have been investigated extensively and found to have a beneficial effect on the flow.

In own numerical investigations concerning the application of end wall contouring [40] and fillets [41] to the rotor of the radial turbine [17] the best results were obtained by use of fillets.

B. Side wall corrections in the mixed flow rotor

To demonstrate the usefulness of side wall corrections the flow behaviour on the suction side of a mixed flow rotors blade is visualized at an overload operating point for a blade design without (a) and with side wall corrections (b) applied,

Fig. A. The colour scale visualises the non-dimensional blade wall shear coefficient c_f in main flow direction y

$$c_f \equiv \frac{\tau}{\frac{\rho}{2} w_\infty^2} \quad (\text{a})$$

with the wall shear stress τ at the blade and the freestream velocity w_∞ approaching the blade. The thin black lines visualize the velocity streamlines near the blade surface. c_f values of approximately zero indicate flow separation. When separated regions approaching the leading edge (LE) the flow on the blade stalls, hence the torque produced by the blade collapses suddenly. Obviously with side wall corrections applied the regions of separated flow propagate less compared to the uncorrected blade. Integral values determined from the CFD analysis demonstrated an increase in peak efficiency of about $\eta_{ts} = 1\text{-}2\%$ and a remarkable extension in maximum flow rate before stall of $\Delta\phi_{mp} \approx 30\%$ under inwards flow.

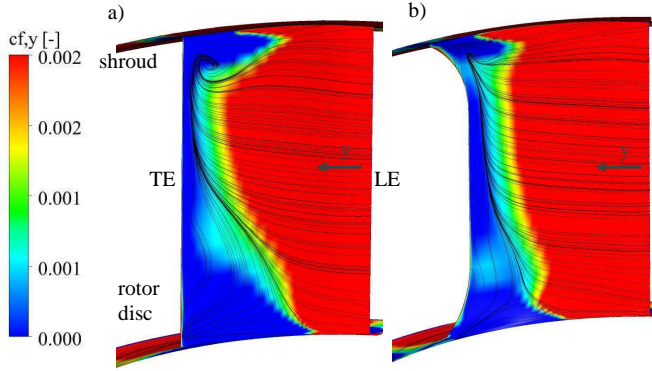


Fig. A. Effect of side wall correction on separated flow on blade suction side; a) standard blade (NoSWC), b) blade with side wall correction (SWC)

As the expansion of secondary flows in corners is known to diminish with decreasing thickness of the boundary layer, and hence with increasing Reynolds number, a useful approach to scale the dimensions of the corrections applied at model turbines to full scale application could be the scaling by means of the expected local boundary layer thickness. An obvious attempt is to refer the dimensions of the side wall corrections to the boundary layer thickness at the blade instead of the chord length. An analytic estimate to determine the boundary layer thickness δ at flat plate is introduced in [31]

$$\delta = 0.14 \frac{\nu}{u_D} \frac{Re_L}{\ln Re_L} G(\ln Re_L). \quad (\text{b})$$

$G(\ln Re)$ is a function little depending on $\ln Re$, with the limit value of one for $\ln Re \rightarrow \infty$. In the relevant range for this study of $10^5 \leq Re_L \leq 10^6$ $G \approx 1.5$. The dimensions of the side wall corrections applied to the mixed flow rotor referred to the boundary layer thickness are compiled in Table IV.

TABLE IIIV
ROTOR SIDE WALL CORRECTIONS REFERRED TO THE BOUNDARY LAYER THICKNESS

A rotor disc region		at shroud region	
$\Delta b_{I-IV}/\delta [-]$	9	$\Delta b_{III-IV}/\delta [-]$	10
$\Delta t_{I-IV}/\delta [-]$	0	$\Delta t_{III-IV}/\delta [-]$	0
$\Delta LE_{I-IV}/\delta [-]$	0	$\Delta LE_{III-IV}/\delta [-]$	0
$\Delta TE_{I-IV}/\delta [-]$	4.2	$\Delta TE_{III-IV}/\delta [-]$	6.3

C. Uncertainty in measurements

The uncertainties of measurements at the test rig are determined according to EDEN [42], DIN 1319-3 [43] and DIN 1319-4 [44] (equivalent to the European standard EN 13005). The cumulated uncertainties of the aerodynamic coefficients at discrete operating points at peak efficiency ('opt') and maximum power ('mp') for the mixed flow turbine are compiled in Table V. These values are determined using the random errors specified for the test rigs measurement equipment (for more details see. [25]). Bias uncertainties in the aerodynamic coefficients are minimized due to the following actions:

- the layout of the test rig and positioning of the instrumentation according to ISO 5801 [23],
- continuous monitoring and correction of zero offsets,
- careful calibration of the volume flow rate Venturi nozzle,
- air densities correctly determined at each reference plane,
- direct telemetric torque measurement between rotor and generator shaft excluding bearing losses ($\eta_{mech} = 100\%$) and hence neglected.

TABLE V
RELATIVE AERODYNAMIC MEASUREMENT UNCERTAINTIES AT DISCRETE OPERATING POINTS OF THE MIXED FLOW TURBINE

Operating point	$U_{C,rel,\phi} [\%]$	$U_{C,rel,\psi} [\%]$	$U_{C,rel,\lambda} [\%]$	$U_{C,rel,\eta} [\%]$	
inwards	opt	0.69	0.84	0.76	1.32
	mp	0.70	0.68	0.75	1.23
outwards	opt	0.72	0.99	0.98	1.58
	mp	0.85	0.69	0.77	1.34

Exemplary, an efficiency curve with errors band (red) at each measurement point is depicted for the outward flow direction of the mixed flow turbine in Fig. C. Within the efficiency curve all relevant uncertainties of ϕ , ψ and λ are included.

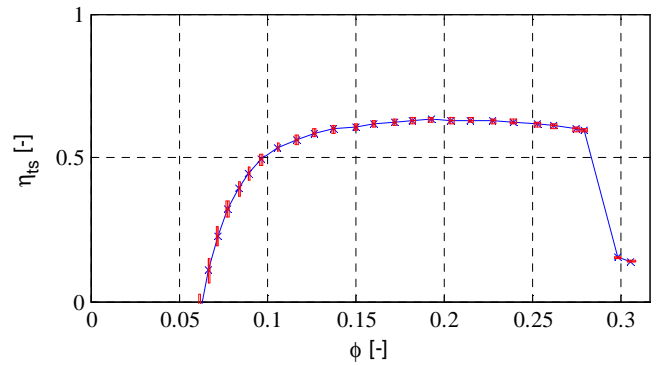


Fig. C. Exemplary efficiency curve for the mixed flow turbine under outward flow with error band

Based on the acoustic measurement method employed, the cumulated uncertainty regarding the overall sound power level is estimated to $U_{C,LW} = 2$ dB.